

## Article

# Distance-Based Analysis of Early Fire Indicators on a New Indoor Laboratory Dataset with Distributed Multi-Sensor Nodes

Pascal Vorwerk <sup>1,\*</sup> , Jörg Kelleter <sup>2</sup>, Steffen Müller <sup>2</sup> and Ulrich Krause <sup>1</sup> 

<sup>1</sup> Faculty of Process- and Systems Engineering, Institute of Apparatus and Environmental Technology, Otto von Guericke University of Magdeburg, Universitätsplatz 2, 39106 Magdeburg, Germany

<sup>2</sup> GTE Industrieelektronik GmbH, Helmholtzstr. 21, 38–40, 41747 Viersen, Germany

\* Correspondence: pascal.vorwerk@ovgu.de

**Abstract:** This work analyzes a new indoor laboratory dataset looking at early fire indicators in controlled and realistic experiments representing different incipient fire scenarios. The experiments were performed within the constraints of an indoor laboratory setting using multiple distributed sensor nodes in different room positions. Each sensor node collected data of particulate matter (PM), volatile organic compounds (VOCs), carbon monoxide (CO), carbon dioxide (CO<sub>2</sub>), hydrogen (H<sub>2</sub>), ultraviolet radiation (UV), air temperature, and humidity in terms of a multivariate time series. These data hold immense value for researchers within the machine learning and data science communities who are keen to explore innovative and advanced statistical and machine learning techniques. They serve as a valuable resource for the development of early fire detection systems. The analysis of the collected data was carried out depending on the Manhattan distance between the fire source and the sensor node. We found that especially larger particles (>0.5 μm) and VOCs show a significant dependency with respect to the intensity as a function of the Manhattan distance to the source. Moreover, we observed differences in the propagation behavior of VOCs, PM, and CO, which are particularly relevant in incipient fire scenarios due to the presence of strand propagation effects.

**Keywords:** early fire detection; multi-sensor network; data-driven fire detection; machine learning; public dataset



**Citation:** Vorwerk, P.; Kelleter, J.; Müller, S.; Krause, U. Distance-Based Analysis of Early Fire Indicators on a New Indoor Laboratory Dataset with Distributed Multi-Sensor Nodes. *Fire* **2023**, *6*, 323. <https://doi.org/10.3390/fire6080323>

Academic Editor: Grant Williamson

Received: 6 June 2023

Revised: 25 July 2023

Accepted: 17 August 2023

Published: 18 August 2023



**Copyright:** © 2023 by the authors. Licensee MDPI, Basel, Switzerland. This article is an open access article distributed under the terms and conditions of the Creative Commons Attribution (CC BY) license (<https://creativecommons.org/licenses/by/4.0/>).

## 1. Introduction

The increasing availability of (low-cost) sensor technology has resulted in high amounts of data available for numerous processes [1–4]. Advancements in computing technology, particularly in the realm of smart computing, have enabled the processing of large volumes of data to extract crucial information. As a result, these data can now be accessed in near real time. Consequently, it has become possible to continuously monitor complex systems, such as the occurrence of fires in buildings [5–10]. Multi-sensor approaches have shown promising potential in early fire detection, particularly when compared to traditional smoke alarm devices [11].

In recent decades, the interest in developing machine-learning-based fire detection solutions has grown significantly to handle the expanding volume of multi-sensor data [5,12]. However, there is still a scarcity of available real fire datasets for model building and validation [11,13,14] due to the high associated costs. One drawback of the existing real fire datasets is the lack of diverse distances between sensors and the location of the fire source since multi-sensor fire detection systems are constrained to a specific detection area [6].

Previous studies have predominantly employed a single sensor placed on the ceiling of a fire test room, coupled with a fixed position for the fire source [11,14–16]. In some other studies, the propagation effects were limited by using small room sizes [6,17]. Gutmacher et al. [18] investigated the differences in the propagation behavior of smoke

particles and gases in various EN54 standard test fires. The authors utilized a multi-sensor array and commercial smoke detectors to measure CO, NO<sub>2</sub>, humidity, temperature, and smoke density. The authors identified a research gap in the examination of the varying propagation behavior of gases and smoke during (incipient) fire scenarios.

Considering the inherent difficulty in accurately determining the location of a fire source [19,20] and the resulting distance between the fire origin and the sensor in real-world fire detection applications, it is crucial for models to be robust against such uncertainty.

To fully harness the potential of multi-sensor measurements, encompassing gases, vapors such as VOC, and PM as early fire indicators, it is imperative to develop a comprehensive understanding of how these sensor measurements interact in various incipient fire scenarios and at different distances from the fire source [21].

In this work, we provide and analyze a new dataset that allows for model building and validation at various sensor node positions in a standard EN54 test room using a multi-sensor node network. For the first time, this enables the consideration of strand propagation effects during the initial stages of various incipient fires within a real fire dataset.

The subsequent sections of this paper introduce the experimental setup utilized in this study. Following that, we examine the behavior of sensor measurements, including PM, VOC, CO, CO<sub>2</sub>, H<sub>2</sub>, UV, air temperature, and humidity. Specifically, we focus on their dispersion characteristics and the time it takes for them to become relevant as early fire indicators in various incipient fire scenarios. In conclusion, we assess the usability of the investigated early fire indicators in terms of their robustness to position dependency and their contribution to achieving the earliest possible detection.

## 2. Related Work

A variety of different sensor measurements were used in terms of “fire parameters” [22] for (early) fire detection in the previous literature. In the context of this paper, we propose the use of the term “early fire indicators” in the sense of direct sensor measurements derived from a multi-sensor network for detecting incipient fires at early stages. Additional early fire indicators that are model-based (e.g., trend features) are part of additional work.

In previous studies, a combination of CO and CO<sub>2</sub> was used in the sense of early fire indicators [11,15,17].

Other works proposed using air temperature, humidity, and smoke concentration in addition to CO and CO<sub>2</sub> [5,16].

Wu et al. [5] argued that CO<sub>2</sub> and humidity are relevant “byproducts” of combustion processes but excluded these measurements in their work since they are highly affected by environmental changes and, therefore, prone to false positives.

Solórzano et al. [11] used H<sub>2</sub>, as well as methane (CH<sub>4</sub>), nitrogen oxides (NO<sub>x</sub>), and VOCs, as an additional early fire indicator. The authors found that early emissions of incipient fires (smoldering fires) include high levels of CO and VOCs. The authors stated the importance of measuring VOCs within a multi-sensor approach for detecting fires at a very early stage [11]. This finding was confirmed by Nazir et al. [14], who used total volatile organic compounds (TVOCs), in addition to air temperature, humidity, CO<sub>2</sub>, and ammonia (NH<sub>3</sub>), as early fire indicators.

Krüger et al. [23] found that the smoldering process of different polymeric materials commonly found in households (wood, PUR foam, and PE) releases significant amounts of H<sub>2</sub> in the initial stages of a fire, even before detectable amounts of CO and smoke are released. The authors suggested utilizing a combination of H<sub>2</sub> sensors and additional sensors (e.g., smoke detectors) for improved detection results.

This finding was confirmed by Hayashi et al. [24]. The authors measured significant quantities of H<sub>2</sub> released by a smoldering fire of cotton in an unventilated (10 × 6 × 3) m<sup>3</sup> test room using a capacitive MEMS hydrogen sensor. Gutmacher et al. [25] identified CO and H<sub>2</sub> to be the most relevant gases for detecting smoldering fires.

As pointed out by Rachman et al. [6], multi-sensor fire detection systems have limitations in terms of the detection area. To address this, the authors suggested employing multiple sensor nodes within a single room to enhance the detection area and increase the sensor sensitivity for the specific application room. The authors placed a total of eight sensor nodes in every corner of a rectangular test room. Each sensor node contained a “[...] fire sensor, smoke sensor, and temperature sensor” [6], which were not specified in more detail. However, the size of the test room was very small— $(50 \times 50 \times 60) \text{ cm}^3$ —which is why it is questionable whether the authors were able to detect relevant differences in the propagation behavior of the sensor measurements.

### 3. Materials and Methods

#### 3.1. Sensor Network Setup

The sensor network setup is depicted in Figure 1. Each sensor node consisted of sensors controlled by a microcontroller (ESP32). Communication between the microcontroller and a broker/server occurred over WiFi using the MQTT protocol. The server was a physical Raspberry Pi.

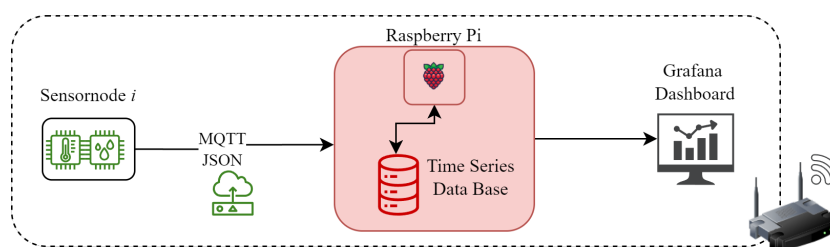


**Figure 1.** Sensor network architecture for the experimental setup.

The microcontroller sent the sensor data in the form of a JSON to the Raspberry Pi, where a Python script decoded the JSON and wrote the sensor data into an Influx time-series database, where an UTC timestamp is automatically assigned to each measuring point.

Measurement data were exported from the Influx time-series database as a CSV file using a Python script. For real-time monitoring of the sensor data during the experiments, a Grafana dashboard was used. Each node in the network contained the sensors listed in Table 1.

**Table 1.** Overview of sensors in each sensor node.

| Sensor     | Manufacturer | Measurand                          | Unit             |
|------------|--------------|------------------------------------|------------------|
| SPS30      | Sensirion    | PM                                 | $\text{cm}^{-3}$ |
| SVM40      | Sensirion    | VOC                                | A.U.             |
| CO/MF-1000 | MEMBRAPOR    | CO                                 | ppm              |
| UST6xxx    | UST          | H <sub>2</sub>                     | ppm              |
| SCD40      | Sensirion    | CO <sub>2</sub>                    | ppm              |
| UVTRON     | HAMAMATSU    | UV photon                          | #                |
| SGP40      | Sensirion    | Temperature, relative air humidity | °C, %            |

We used the UST6xxx sensor array containing the GGS 6530 T gas sensor element from the manufacturer UST in order to ensure low cross-sensitivity to CH<sub>4</sub>, CO, and alcohol. The UST6xxx is nearly insensitive to CH<sub>4</sub> exposure up to 1000 vppm at a heating temperature of 475 °C [26].

The sampling rate was restricted by two main factors. The first limitation is due to the internal processes of the sensors used. The CO/MF-1000 sensor has a T90 response time of about 25 s, meaning that 90% of the exposed gas concentration is recorded in less than 25 s [27]. The UST6xxx utilizes internal temperature cycles with a 10 s interval for H<sub>2</sub> gas detection [26]. Therefore, a sampling rate >1 sample per 10 s would not provide

any further information. The second limitation is due to the propagation behavior of combustion products during incipient fires with low heat release rates, as investigated in this study. Changes in gas concentrations due to different stages of combustion processes experience the inertia of propagation effects in a non-ventilated room environment. These changes occur on the order of minutes rather than seconds, as observed in the findings of Gutmacher et al. [25]. Considering these factors, a sampling rate of 1 sample per 10 s was employed in this research.

According to Rachman et al. [6], we employed a sensor network using various distributed sensor nodes in our experimental setting. The network consisted of 9 sensor nodes (0008-0016) that were positioned around the fire source, as shown in Figure 2.

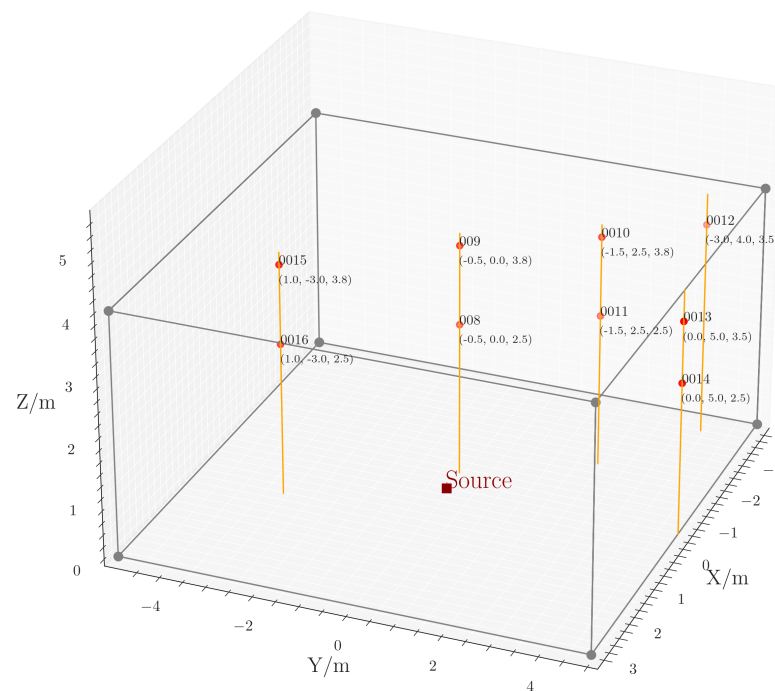


**Figure 2.** Positions of the fire source and sensor nodes in the EN54 fire test room.

All experiments were conducted in a non-ventilated EN54 fire test room with dimensions of  $(7 \times 10 \times 4) \text{ m}^3$ . The positions of the sensor nodes in the fire room resulted in various distances (Euclidean and Manhattan) with respect to the fire source, as depicted in Table 2.

**Table 2.** Positions and distances of sensor nodes and the source within the test room.

| Sensor_ID | x<br>(m) | y<br>(m) | h<br>(m) | Euclidean<br>(m) | Manhattan<br>(m) |
|-----------|----------|----------|----------|------------------|------------------|
| 0008      | -0.5     | 0.0      | 2.5      | 2.5              | 3.0              |
| 0009      | -0.5     | 0.0      | 3.8      | 3.8              | 4.3              |
| 0010      | -1.5     | 2.5      | 3.8      | 4.8              | 7.8              |
| 0011      | -1.5     | 2.5      | 2.5      | 3.8              | 6.5              |
| 0012      | -3.0     | 4.0      | 3.5      | 6.1              | 10.5             |
| 0013      | 0.0      | 5.0      | 3.5      | 6.1              | 8.5              |
| 0014      | 0.0      | 5.0      | 2.5      | 5.6              | 7.5              |
| 0015      | 1.0      | -3.0     | 3.8      | 4.9              | 7.8              |
| 0016      | 1.0      | -3.0     | 2.5      | 4.0              | 6.5              |

In order to achieve a more precise evaluation of the plume-shaped propagation behavior, we opted for the Manhattan distance over the Euclidean distance. The Manhattan distance considers the varying x–y distances between sensor nodes 0009 (positioned above

the source) and 0011 (or 0016) and the source itself. While the Euclidean distance may yield similar values for these nodes, the Manhattan distance provides a more precise representation of the propagation behavior of the released products by accurately capturing the varying x–y distances from the source.

### 3.2. Experimental Procedure

The conducted experiments can be categorized into fire scenarios, nuisance scenarios, and background measurements, as summarized in Table ??.

**Table 3.** Overview of the experiments carried out looking at the termination criterion and the number of experiments.

| Scenario   | Termination Criterion        | Number of Experiments |
|------------|------------------------------|-----------------------|
| Wood       | Max. Duration of Experiment  | 3                     |
| Candles    | Max. Duration of Experiment  | 3                     |
| Cable      | Max. Duration of Experiment  | 3                     |
| Lunts      | Max. Duration of Experiment  | 3                     |
| Ethanol    | Sample Completely Evaporated | 3                     |
| Deodorant  | Two Sprays of 15 s           | 2                     |
| Hairspray  | Two Sprays of 15 s           | 1                     |
| Background | -                            | -                     |
|            |                              | Total: 18             |

The experimental series consisted of 4 fire experiments as shown in Figure 3, 3 nuisance experiments, and multiple background measurements between the fire and nuisance experiments. The fire experiments were carried out as detailed below.

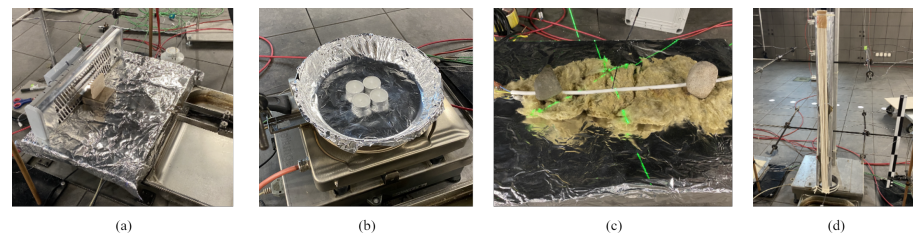


**Figure 3.** Setup of carried out fire experiments; (a) wood, (b) candles, (c) cable, (d) lunts.

**The wood fire** was performed with a piece of beech wood with dimensions ( $6 \times 8 \times 0.9$ )  $\text{cm}^3$  and a quartz radiant heater (“HQH 1200/3/1”) from the company “ROWI” with a heating capacity of 1200 W. The quartz radiant heater was positioned at a distance of 5 cm from the vertical beech wood. With this test arrangement, a wood smoldering fire was simulated. Flaming combustion was not triggered. The average wood moisture content was approx. 5%. The prepared beech wood pieces were stored dry under standard conditions prior to the experiments. The wood samples had a mean mass of 30.8 g before starting the experiment procedure.

**The candle fire** was performed with four commercially available tea lights (100% paraffin, housing included), which were placed on a heating plate. The mean mass of the four candles was 47.63 g. To accelerate the melting process, the heating plate was heated to a constant temperature of 450 °C approx. 30 s after lighting the tea lights.

**The cable fire** was performed with a halogen-free NHXMH-type cable (length = 35 cm) from the manufacturer “Lapp Group”. The fire was triggered by an electrical overload of approx. 130 A DC. The cable was insulated on the lower side with rock wool.

**The lunt fire** was performed with eight lunts of cotton material (diameter = 4 mm) from the manufacturer “Fehr-Erlen”. The average mass of the 8 fuses before the start of the

experiment was 200.40 g. The lunts were arranged annularly and ignited using a heating coil with a surface temperature of approx. 600 °C.

After the fire experiments, nuisance measurements were performed to create a set of non-fire data.

**Ethanol** was evaporated from a vat above the heating plate. For this purpose, the hot plate was heated to 50 °C. A total volume of 10 ml ethanol per experiment was completely evaporated.

**Deodorant** was sprayed evenly into the room by means of two 15 s sprays. We used deodorant from the manufacturer “elkos” without aluminum salts.

**Hairspray** was sprayed in a similar manner to the deodorant with two sprays of 15 s. We used hairspray from the manufacturer “Schwarzkopf”, type “3 Wetter taft ULTRA 4”.

**The background** was measured between the nuisance/fire experiments for a minimum measurement time of one hour. The background measurement started when the ventilation of the test room had been completed and a minimum waiting time of 30 min had passed.

### 3.3. Dataset

The dataset contains 305,304 rows and 16 columns in total and is structured as a continuous multivariate time series. Each row contains all measurements of one unique sensor node at a unique time stamp. The columns represent the sensor measurements explained in Table A1.

The data are labeled with four types of labels: a scenario-specific label (“scenario\_label”); a binary label (“anomaly\_label”), which distinguishes between a “Normal” state (background) and an “Anomaly” (fire or nuisance scenario); a ternary label (“ternary\_label”) distinguishing between “Nuisance”, “Fire”, and “Background”; and a progress label (“progress\_label”) that can be used to divide the sequences of events into subsequences depending on the ongoing physical subprocesses.

The dataset contains 82.98% background data points and 17.02% anomaly data points, which can be divided into 12.50% data points of fire anomalies and 4.52% data points of nuisance anomalies.

## 4. Results

The response behavior of the sensor measurements was evaluated based on two criteria. The first criterion involved determining the maximum absolute value of each measurement, considering the scenario and the Manhattan distance from the source (as discussed in Section 4.1). The second criterion involved analyzing the time difference between the start of the experiment and the time point at which a defined threshold was reached, taking into account the scenario and the Manhattan distance from the source (as described in Section 4.2).

It should be noted that Figures 4–6 include data points from two sensor nodes at Manhattan distances of 7.8 m and 6.5 m, respectively. This is because sensor nodes 0010 and 0015, and sensor nodes 0011 and 0016 share the same Manhattan distance from the source, as indicated in Table 2.

### 4.1. Intensity Dependence

Figure 4 depicts the maximum values obtained for each sensor measurement, taking into account both the scenario and the Manhattan distance from the source. Generally, a noticeable decrease in intensity was observed with an increasing Manhattan distance between the sensor node and the source.

However, there were some notable exceptions observed for the CO<sub>2</sub>, humidity, UV, and PM<sub>05</sub> measurements. During the conducted fire experiments, which predominantly involved incomplete combustion, only small amounts of CO<sub>2</sub> were released, leading to minimal impact on the CO<sub>2</sub> measurement.

One exception to this trend was observed in the candle scenario, where a more complete combustion took place, leading to higher levels of CO<sub>2</sub> release. Interestingly, in the candle scenario, the dispersion of CO<sub>2</sub> appeared to be nearly independent of the distance between the source and the sensor. However, the humidity remained largely unaffected by the conducted experiments, exhibiting no discernible trend in relation to the distance from the source.

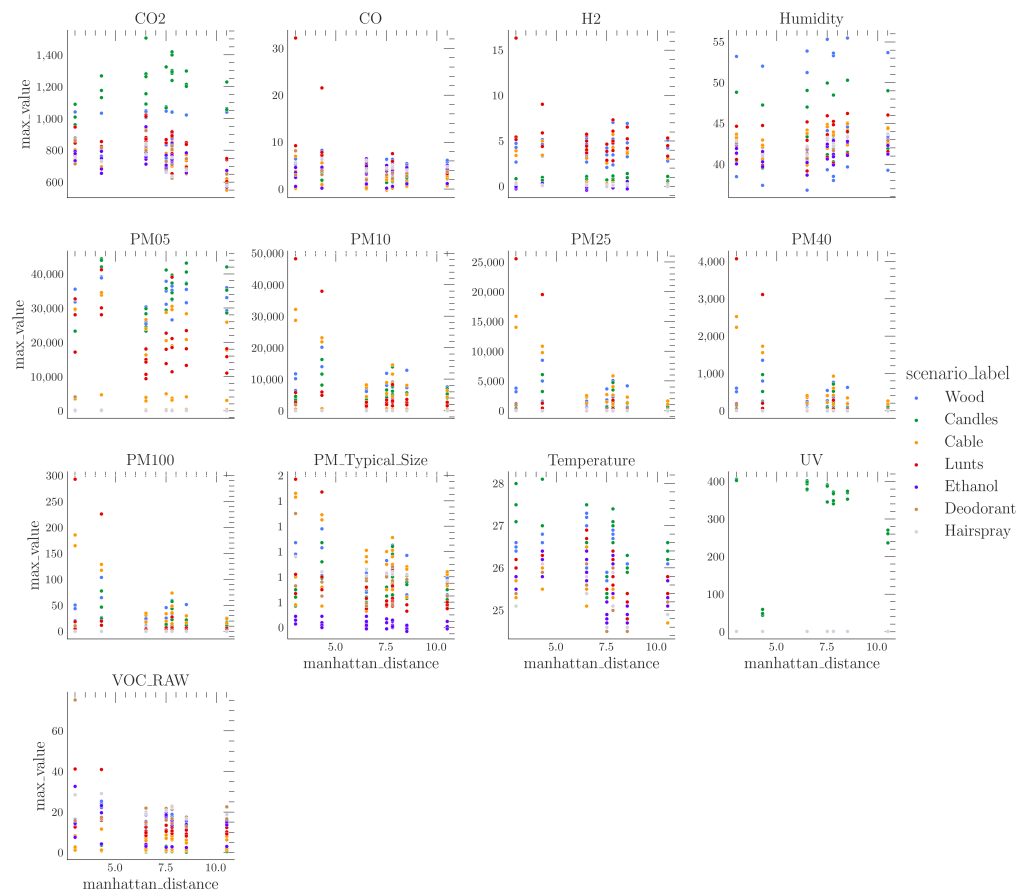


**Figure 4.** Absolute maximum values for each sensor measurement depending on the Manhattan distance from the source and the scenario.

By analyzing the UV measurements, two noteworthy conclusions could be drawn. Firstly, UV signals were exclusively detected in the candle scenario, which was the only scenario characterized by flaming combustion. This indicates that UV measurements can serve as a reliable indicator for scenarios involving open flames. Secondly, the maximum values of the UV measurements were nearly unaffected by the Manhattan distance from the source. This can be attributed to the absence of any objects within the room that would obstruct the “line of sight” between the sensor node and the source, allowing the UV signals to propagate freely regardless of the distance. One exception could be observed at a Manhattan distance of 4.3 m (sensor node 0009), where the UV signal dropped from 400 to around 100 counts. This is due to the presence of sensor node 0008, which was positioned directly below sensor node 0009 at a height of 2.5 m. Since “the line of sight” between sensor node 0009 and the source was totally vertical, the “line of sight” was significantly affected by sensor node 0008.

The air temperature exhibited a minor decline as the distance from the source increased, albeit within a narrow range of 24 °C to 28 °C. This observation can be attributed to the nature of the conducted fire scenarios, which mainly involved fires in their initial stages with low heat release rates. As a result, the impact on the surrounding air temperature was only marginal.

VOC showed a noticeable correlation with the Manhattan distance. It can be seen in Figure 4 that VOC was released in the lunt, cable, and wood scenarios, as well as in all nuisance scenarios involving ethanol, deodorant, and hairspray. However, VOC was not detected in the candle scenario.

Remarkably, PM exhibited distinct behavior: smaller particles (PM05) showed minimal sensitivity to the Manhattan distance, while the count of larger particles (PM10–PM100) decreased as the Manhattan distance increased. Two primary factors contribute to this pattern, namely, agglomeration and gravitational settling, as discussed by Mostafa et al. [28].

Agglomeration refers to the process by which particles stick together, forming larger clumps of particles. Agglomeration can result in the formation of particles that are too large to remain suspended in the air, leading to a decrease in the concentration of PM [29].

The extent to which gravitational settling affects particles depends on their size and density. Larger particles tend to have higher sedimentation velocities than smaller particles, and the effect of gravity on smaller particles is relatively less significant in terms of their propagation behavior, as stated by Mostafa et al. [28]. From this, we can conclude that smaller particles are more influenced by air movement, and their behavior is not primarily affected by agglomeration. This was evident, as we would have observed the opposite pattern, i.e., a decrease in the number of smaller particles and a less noticeable decrease in the number of larger particles with an increasing Manhattan distance from the source, if agglomeration were the primary influencing factor.

In our study, the effect of gravitational settling appears to be the primary determinant of particle propagation, as there were no external influences such as forced ventilation or significant temperature variations within the test room. The larger particles tended to move closer to the ground due to gravity, leading to less frequent detection by the more distant sensor nodes.

Furthermore, we made an intriguing observation regarding the sensor nodes positioned at the same height (2.5 m) and with an equal Manhattan distance from the source (sensor node 0011 and sensor node 0016, both at a Manhattan Distance of 6.5 m) but located at different positions in the x–y direction of the room. Within a given fire scenario, these nodes exhibited slightly varied maximum values for each measurement. A specific example can be seen in the wood scenario illustrated in Figure 5. It can be seen that sensor node 0011 recorded slightly higher maximum values for CO and all PM (excluding PM05) while measuring lower maximum values for VOC than sensor node 0016.

When comparing sensor nodes 0015 and 0010 (Manhattan distance = 7.8 m, height = 3.8 m) positioned directly above sensor nodes 0016 and 0011, a slightly different behavior could be observed. Sensor node 0010 measured higher values of PM (excluding PM05) and VOCs than sensor node 0015. This behavior is consistent with that of sensor nodes 0016 and 0011, which were located below, except for the PM05 measurement. Figure 4 indicates that PM05 does not exhibit a clear dependence on the distance from the source in general, suggesting that the exception here may be due to random variation in propagation behavior.

However, when it comes to the CO measurement, sensor node 0010 registered slightly lower maximum values than sensor node 0015, which contrasts with the behavior of sensor nodes 0016 and 0011 (where sensor node 0011 measured higher maximum CO values than sensor node 0016). Given the absence of external ventilation effects and consistent temperature conditions within the test room, we can infer that different factors influence the propagation behavior of combustion products. PM and VOCs seem to propagate uniformly, but CO behaves differently.

One possible explanation is that the VOCs released during combustion processes primarily consist of vapor components, as stated in [30,31]. Similar to PM, these components are heavier than pure gases and likely disperse differently from the released gaseous components. It is plausible that multiple dispersion patterns occur, with some strands primarily containing gases and others containing VOCs and larger particles.

The central assumption is that VOCs, PM, and gases (such as CO) form distinct strands during the combustion process, potentially at different stages of the combustion process.

It should be noted that these strands are not composed solely of a single component but rather have a predominant presence of a particular component.

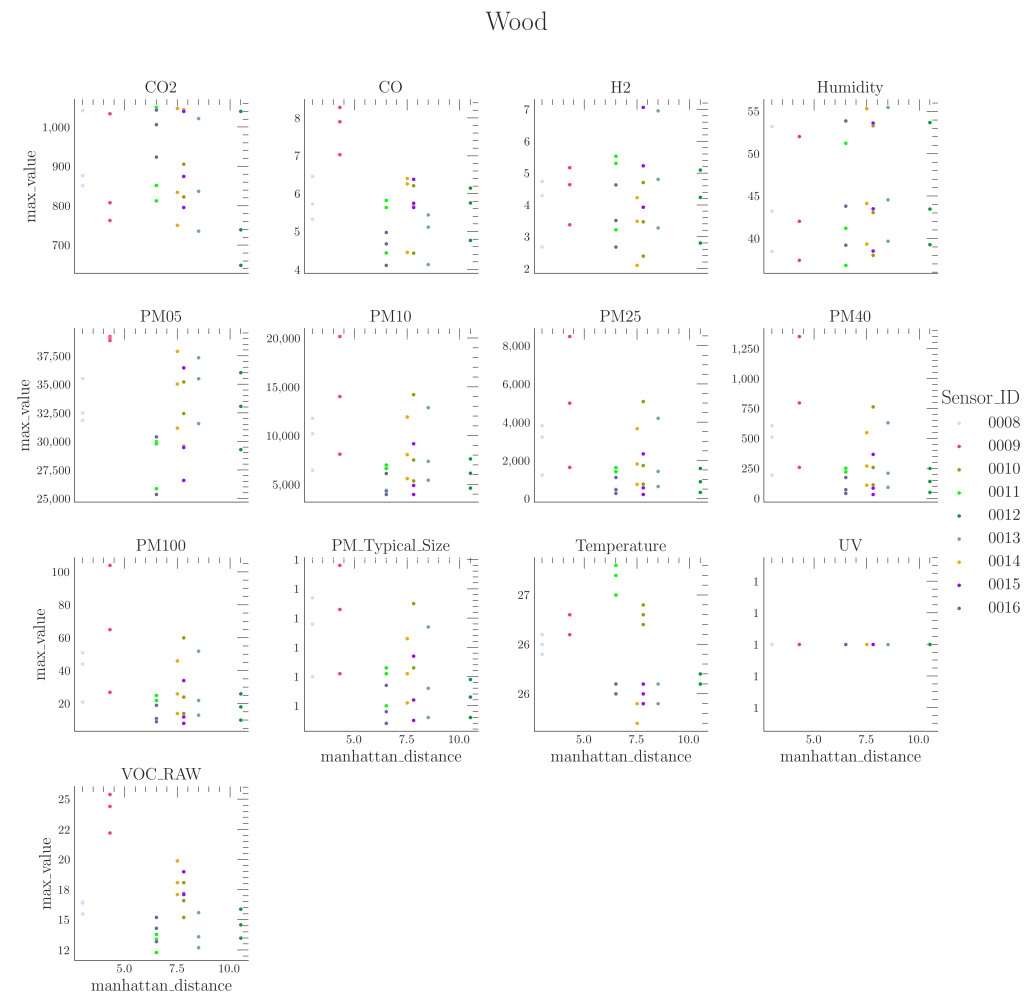


**Figure 5.** Absolute maximum values for each sensor measurement depending on the Manhattan distance from the source and the Sensor\_ID within the wood scenario.

#### 4.2. Time Dependence

In order to examine the time delay associated with different sensor node positions, a global threshold was established for each sensor measurement. The threshold values are outlined in Table 4.

The determination of the thresholds involved a prior analysis of the collected time-series data. The aim was to establish values that would only be surpassed by exceptional peaks associated with specific experiments, ensuring robustness. At the same time, the thresholds were set as low as possible to enable detection, even at sensor nodes located far from the emission source, thereby enhancing sensitivity.

**Table 4.** Global thresholds for every sensor measurement.

| Measurand       | Global Threshold | Unit             |
|-----------------|------------------|------------------|
| CO <sub>2</sub> | 1200             | ppm              |
| CO              | 2                | ppm              |
| H <sub>2</sub>  | 1.5              | ppm              |
| Humidity        | 75               | %                |
| PM05            | 100              | cm <sup>-3</sup> |
| PM10            | 75               | cm <sup>-3</sup> |
| PM25            | 75               | cm <sup>-3</sup> |
| PM40            | 75               | cm <sup>-3</sup> |
| PM100           | 10               | cm <sup>-3</sup> |
| PM_Typical_Size | 0.55             | μm               |
| Temperature     | 30               | °C               |
| UV              | 3                | #                |
| VOC_RAW         | 2.5              | A.U.             |

The thresholds were applied using a rule-based baseline model. They were set globally, irrespective of the scenario or the position of the sensor node. This decision was made because, in real-world applications, the specific scenario and the distance between the sensor node and the emission source are typically unknown [14].

The time delay, denoted as  $\delta t$ , was calculated based on Equation (1):

$$\delta t = t_{detect} - t_0 \quad (1)$$

where  $t_0$  is the time point when the experiment started, and  $t_{detect}$  is the time point when the global threshold was exceeded for the first time after the start of the experiment. The results are shown in Figure 6.

The time lag between the experiment onset and the threshold exceedance must not be seen as a direct measure of the fire detection time. This is due to the experimental design (see Section 3.2), which aimed to represent the early stages of an ongoing incipient fire. This is why several minutes elapsed between the experiment onset and the release of the first combustion products when the fire material was sufficiently thermally conditioned. However, in order to compare the time dependence of the examined fire indicators, the official start of the experiment was conducted as  $t_0$ , resulting in relatively high time deltas in general.

The thresholds of humidity and air temperature were not exceeded at all, which is why they are not visible in Figure 6. As mentioned in Section 4.1, the maximum values of these two measurements did not exhibit any correlation with the distance from the source. This finding confirms that the carried out experiments had minimal impact on humidity and air temperature in general, which contradicts the findings of Wu et al. [5] and Nakip et al. [16], who suggested using humidity and air temperature as relevant early fire indicators.

Another noteworthy observation is that the thresholds for the UV and CO<sub>2</sub> measurements were only exceeded in the candle scenario, which exclusively involved flaming combustion and a complete combustion process.

For the lunt and cable scenarios, we observed a consistent increase in the time delta as the Manhattan distance increased for all measurements, except for UV.

In the wood scenario, a significant time delay for the H<sub>2</sub> measurement was observed. In fact, it took up to half an hour from the start of the experiment for the sensor nodes closest to the emission source to exceed the threshold. This time delay was considerably longer than that in the cable and lunt scenarios.

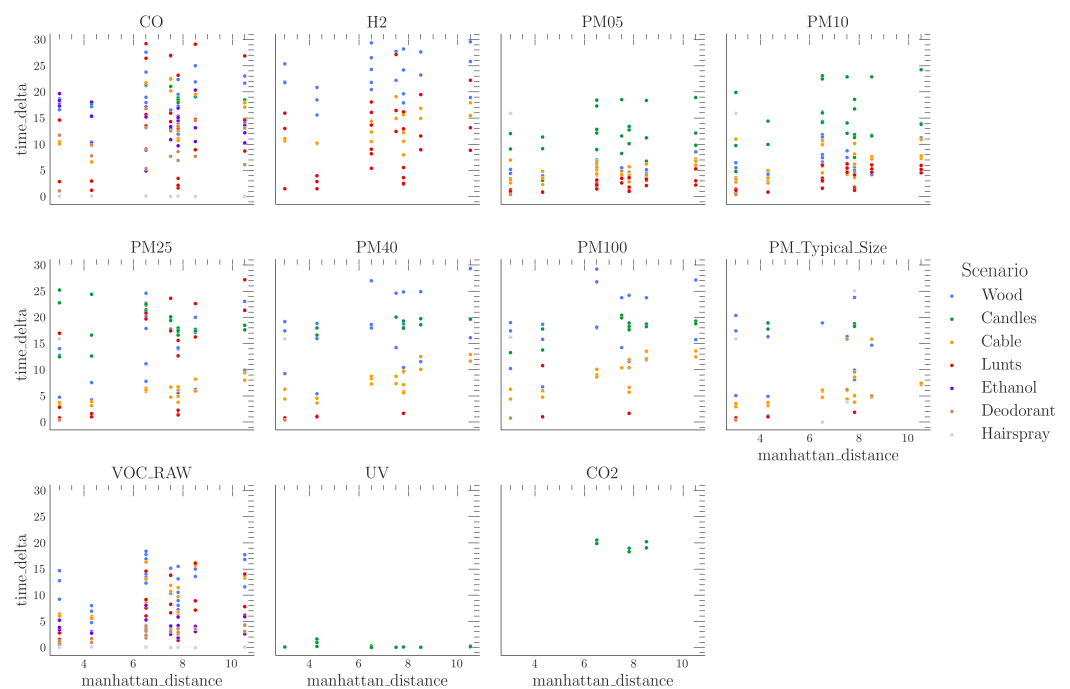


**Figure 6.** Time delta (in min) between start of experiment and threshold exceedance for each sensor measurement depending on the Manhattan distance from the source and the scenario.

The observed delay can be attributed to the exclusive production of  $H_2$  during the glowing process [32], which occurred towards the end of the wood experiment. The formation of  $H_2$  is a consequence of the water–gas shift reaction described in Equation (2) [33]:



In the lunt scenario, the glowing process initiated at the beginning of the experiment, leading to the shortest time delta (ranging from 2 to 9 min, depending on the Manhattan distance) for the  $H_2$  threshold to be exceeded.

In the cable scenario, a time delta between that of the lunt and wood scenarios was observed for the  $H_2$  measurement, ranging from 10 to 18 min. Again, this can be attributed to the specific experimental procedure. In the lunt scenario, the glowing process initiated right at the beginning of the experiment, leading to the shortest time delta. In the wood scenario, the wood initially underwent carbonization. The process of glowing only started towards the end of the experiment, resulting in the longest time delta. In the cable scenario, the wire of the cable heated up due to electrical overload, leading to the evaporation and carbonization of the insulation. This triggered the glowing process and the release of  $H_2$ . Although the glowing process started earlier than in the wood scenario, it did not occur immediately at the beginning of the cable experiment.

It can be seen in Figure 6 that the time delta of the CO measurement in the wood scenario is similar to that of the  $H_2$  measurement, albeit slightly shorter. This suggests that the presence of a significant amount of CO facilitates the release of  $H_2$  during the glowing process, as described by the reaction in Equation (2).

When examining PM, it is evident that the smaller particles (PM05 to PM10) in the wood scenario exhibited shorter time deltas than the larger particles (PM25 to PM100). Conversely, in the lunt scenario, PM40 and PM100 did not surpass the threshold beyond a Manhattan distance of 8 m. However, in the wood scenario, these particles did exceed the threshold, albeit with longer time deltas ranging from 16 to 29 min. This phenomenon can be attributed to the use of an external heat source in the wood experiments, as discussed in Section 3.2. The external heat source likely generated stronger thermal buoyancy, enabling

the larger and heavier particles to be transported further away from the emission source in the wood experiments than in the lunt experiments.

In the lunt scenario, VOC exhibited shorter time deltas than the larger particles (>PM10) but slightly longer time deltas than the smaller particles (PM05–PM10). However, the time deltas for VOC were still lower than the measurements of CO and H<sub>2</sub>, and the time deltas between measurements increased the same as the Manhattan distance increased.

The candle scenario stands out due to its complete combustion nature. Only during the transition to wax firing was enough CO<sub>2</sub> produced to surpass the threshold, which explains the time delta of approximately 20 min. CO appeared to be unaffected by the Manhattan distance in terms of reaching maximum values and exceeding the threshold. H<sub>2</sub> did not occur in this particular fire scenario since there was no underlying glowing process.

Regarding PM, PM05 exceeded the threshold the fastest. For all PM sizes, the time delta increased with an increasing Manhattan distance. In contrast to the lunt scenario, the larger particles (PM40 to PM100) exceeded the threshold for all Manhattan distances.

UV exhibited the shortest time deltas among all sensor nodes and remained unaffected by the Manhattan distance. VOC did not surpass the threshold at all.

In the cable scenario, both H<sub>2</sub> and CO took significantly longer to reach the thresholds than all sizes of PM, regardless of the Manhattan distance. Within the PM measurements, smaller particles (PM05) exceeded the threshold slightly earlier than larger particles (PM40 to PM100) at the same Manhattan distance from the source.

## 5. Discussion

In terms of non-gas early fire indicators, we observed that UV and PM05 are the least influenced by the distance between the sensor node and the source within a standard EN54 room size. This makes them the most resilient features against propagation effects that can affect the detection performance.

However, it is important to note that UV is only present in scenarios involving flaming combustion, which is not the case for the majority of incipient fire scenarios [34]. Although the UV signal was clearly seen by all sensors during the flaming combustion in the candle scenario, objects located between the sensor node and the source significantly weakened the signal strength, as shown in Figure 4. Therefore, we propose using UV not directly for ML model construction but rather as an additional rule that can effectively verify fire detection in the case of flaming combustion.

The concentration of larger particles (>PM10) showed a significant dependency on the distance between the sensor and source, resulting in higher time deltas between the experiment onset and threshold exceedance. This is why we propose using only smaller particles (PM05–PM10) as early fire indicators looking at PM.

Regarding VOCs, we observed a clear dependency on the Manhattan distance. VOCs were detected in all fire scenarios, except for the candle fire scenario. While we observed comparable concentrations in all nuisance scenarios, we do not consider VOCs to be a standalone early fire indicator. However, in combination with PM05 and CO, VOCs can be a suitable early fire indicator.

By analyzing the gas-based early fire indicators, we can conclude that CO<sub>2</sub> is only relevant in situations of almost complete combustion. This observation was only made in the candle scenario. Therefore, we can conclude that CO<sub>2</sub> is not a relevant early fire indicator, despite its almost independence from the distance between the source and the sensor node in the case of the candle fire scenario.

CO was emitted in significant quantities across all fire scenarios and exhibited only a minimal dependency on the Manhattan distance. Therefore, we highly recommend considering CO as an essential early fire indicator.

Although H<sub>2</sub> was released only in fire scenarios involving glowing processes, such as the wood and lunt experiments, we propose H<sub>2</sub> as a relevant early fire indicator. This is because glowing processes occur in the majority of incipient fires [35]. The timing of H<sub>2</sub> release varies depending on the specific fire scenario, as discussed in Section 4.2. As

a result, H<sub>2</sub> can be relevant as an early fire indicator either at the very beginning of an incipient fire (as seen in the lunt scenario) or after a certain period of fire development (as seen in the wood scenario).

When used in conjunction with CO, H<sub>2</sub> can enable delimitation to nuisance scenarios, as H<sub>2</sub> was not detected in any nuisance scenario. However, cross-sensitivities of the CO sensor to VOCs led to a significant increase in CO measurement during nuisance scenarios. Given that the time deltas for CO and H<sub>2</sub> were similar in their respective fire scenarios, the simultaneous presence of these two indicators can be considered a reliable feature for early fire detection.

It can be concluded that gas-based sensor measurements and smaller particles (PM<sub>05</sub>–PM<sub>10</sub>) are less affected by the distance between the sensor node and the source than larger particles (>PM<sub>10</sub>) and VOCs. This characteristic makes them less dependent on the physical location of the sensor and more robust as early fire indicators.

However, it should be noted that PM and VOC exhibited the shortest time deltas, particularly in smoldering fire scenarios, including the wood, cables, and lunt scenarios. Although these early fire indicators were more sensitive to the sensor node's position, they became particularly significant during the initial phase of the investigated incipient fire scenarios in this study.

To access the temporal component of the investigated early fire indicators, we measured the time lag between the experiment onset and threshold exceedance (time delta), as discussed in Section 4.2. Due to the experimental design aiming to represent the early stages of incipient fires, we observed relatively high time deltas in general (up to 30 min). This applies particularly to the wood and candle experiments, where several minutes passed before the fire material was thermally decomposed in such a way that the first combustion products were released. In the case of the wood experiment, the piece of wood had to be irradiated with the radiant heater for several minutes before the first decomposition reactions were initialized. In the candle experiment, the wax had to be heated for several minutes with the help of the heating plate until the transition to wax fire took place. Since we aimed to reproduce these transition phases in our experiments, the experimental design was conducted in the proposed way. However, it should be noted that the time delta presented in this work includes the time lag between the start of the experiment and the release of the first combustion products. This resulted in relatively high time deltas, especially for the wood and candle scenarios. Nevertheless, we used the start of the experiment as  $t_0$  in order to ensure the comparability of the time deltas between the different sensor node positions.

## 6. Conclusions and Outlook

This paper presents the results of a series of laboratory experiments conducted with the aim of generating a comprehensive fire dataset that encompasses various incipient fire scenarios in a standard EN54 indoor test room. The primary objective of these experiments was to create a new indoor fire dataset and to evaluate the viability of different sensor measurements as early fire indicators. This serves as an initial feature selection process for the development of machine-learning-based models aimed at detecting the early stages of incipient fires.

We observed a correlation between the Manhattan distance from the source to the sensor node and the response behavior of specific sensor measurements in various incipient fire scenarios. In summary, we found that there is an increase in the time delta of reaching a global threshold respective to the decrease in the measured maximum with an increasing Manhattan distance. However, this correlation is specific to the scenario and the sensor measurement itself.

In summary, our study identified five significant early fire indicators using a multi-sensor approach: H<sub>2</sub>, CO, PM<sub>05</sub>, PM<sub>10</sub>, and VOC. The relevance of these indicators varies depending on the type of incipient fire scenario, as they are released at different stages of the incipient fire. The correlations presented in this paper can be incorporated as

domain knowledge into corresponding models. Furthermore, the knowledge of intensity dependence can enhance the interpretability of model predictions, allowing for a better understanding of how model performance changes at different positions. Moreover, the positional variations captured in this dataset can be utilized to develop more robust models and mitigate the issue of overfitting.

The labeled multivariate time-series dataset offers the opportunity to derive additional features as early fire indicators based on model assumptions. For instance, trend features can be extracted from specific subsequences of the time series, as proposed in Wu et al. [5], which forms part of ongoing work. Furthermore, since the data include timestamps, stream-based approaches can also be modeled. The provided dataset allows for the training and validation of models across different sensor node positions in a room. Additionally, as each fire experiment was conducted three times, the dataset provides an ample number of data points, allowing for the development and evaluation of more complex models compared to previously available datasets.

**Author Contributions:** Conceptualization, P.V. and J.K.; methodology, J.K.; software, P.V.; validation, P.V.; formal analysis, P.V.; investigation, P.V. and J.K.; resources, P.V., J.K., and S.M.; data curation, P.V.; writing—original draft preparation, P.V.; writing—review and editing, J.K. and S.M.; visualization, P.V.; supervision, U.K.; project administration, U.K.; funding acquisition, U.K. All authors have read and agreed to the published version of the manuscript.

**Funding:** The results were generated in the course of the BRAWA research project (BRAWA: Preserving cultural goods through helper motivation and low fire probabilities) that is funded by the German Federal Ministry of Education and Research (BMBF, funding reference numbers 13N15415 and 13N15418) as part of the “Research for Civil Security” program.

**Institutional Review Board Statement:** Not applicable.

**Informed Consent Statement:** Not applicable.

**Data Availability Statement:** The dataset is available in CSV format and can be accessed publicly from the Mendeley Data platform at <https://data.mendeley.com/datasets/npk2zcm85h/1> (DOI: 10.17632/npk2zcm85h.1), accessed on 27 May 2023.

**Conflicts of Interest:** The authors declare no conflict of interest.

## Appendix A. Dataset Description

**Table A1.** Description of the columns in the dataset.

| Column        | Description                      | Format        | Unit                     |
|---------------|----------------------------------|---------------|--------------------------|
| Date          | Index column                     | DatetimeIndex | ‘YYYY-MM-DD<br>hh:mm:ss’ |
| Sensor_ID     | Unique sensor ID                 | string        | [-]                      |
| CO2_Room      | Concentration of carbon dioxide  | float64       | ppm                      |
| CO_Room       | Concentration of carbon monoxide | float64       | ppm                      |
| H2_Room       | Concentration of hydrogen        | float64       | ppm                      |
| Humidity_Room |                                  | float64       | %                        |
| PM05_Room     | Particles < 0.5 $\mu\text{m}$    | float64       | $\text{cm}^{-3}$         |
| PM10_Room     | Particles < 1.5 $\mu\text{m}$    | float64       | $\text{cm}^{-3}$         |
| PM25_Room     | Particles < 2.5 $\mu\text{m}$    | float64       | $\text{cm}^{-3}$         |
| PM40_Room     | Particles < 4.0 $\mu\text{m}$    | float64       | $\text{cm}^{-3}$         |
| PM100_Room    | Particles < 10.0 $\mu\text{m}$   | float64       | $\text{cm}^{-3}$         |

Table A1. Cont.

| Column               | Description  | Format  | Unit |
|----------------------|--|---------|------|
| PM_Room_Typical_Size | Weighted mean of diameter                                    | float64 | µm   |
| Temperature_Room     | Air temperature  | float64 | °C   |
| UV_Room              | UV photon counts   | float64 | #    |
| VOC_Room_RAW         | Volatile organic compounds (raw electrical data from sensor) | float64 | A.U. |
| scenario_label       | experiment specific label                                    | string  | [-]  |
| anomaly_label        | distinguishes between "Anomaly" and "Normal"                 | string  | [-]  |
| ternary_label        | distinguishes between "Nuisance", "Fire", and "Background"   | string  | [-]  |

## References

1. Tsujita, W.; Yoshino, A.; Ishida, H.; Moriizumi, T. Gas sensor network for air-pollution monitoring. *Sens. Actuators B Chem.* **2005**, *110*, 304–311. [[CrossRef](#)]
2. Fireteanu, V.V.; Tudor-Serban, A.; Sacala, I.S.; Moisescu, M.A. Avalanche Prediction Based on Snow Level Monitoring Using Wireless Sensor Networks. *Appl. Mech. Mater.* **2014**, *656*, 369–377. [[CrossRef](#)]
3. Mesquita, E.; Arêde, A.; Pinto, N.; Antunes, P.; Varum, H. Long-term monitoring of a damaged historic structure using a wireless sensor network. *Eng. Struct.* **2018**, *161*, 108–117. [[CrossRef](#)]
4. Dinh, T.L.; Hu, W.; Sikka, P.; Corke, P.; Overs, L.; Brosnan, S. Design and Deployment of a Remote Robust Sensor Network: Experiences from an Outdoor Water Quality Monitoring Network. In Proceedings of the 32nd IEEE Conference on Local Computer Networks (LCN 2007), Dublin, Ireland, 15–18 October 2007; pp. 799–806. ISSN 0742-1303. [[CrossRef](#)]
5. Wu, L.; Chen, L.; Hao, X. Multi-Sensor Data Fusion Algorithm for Indoor Fire Early Warning Based on BP Neural Network. *Information* **2021**, *12*, 59. [[CrossRef](#)]
6. Rachman, F.Z.; Hendrantoro, G.; Wirawan. A Fire Detection System Using Multi-Sensor Networks Based on Fuzzy Logic in Indoor Scenarios. In Proceedings of the 2020 8th International Conference on Information and Communication Technology (ICoICT), Yogyakarta, Indonesia, 24–26 June 2020; pp. 1–6. [[CrossRef](#)]
7. Liang, Y.H.; Tian, W.M. Multi-sensor Fusion Approach for Fire Alarm Using BP Neural Network. In Proceedings of the 2016 International Conference on Intelligent Networking and Collaborative Systems (INCoS), Ostrava, Czech Republic, 7–9 September 2016; pp. 99–102. [[CrossRef](#)]
8. Jana, S.; Shome, S.K. Hybrid Ensemble Based Machine Learning for Smart Building Fire Detection Using Multi Modal Sensor Data. *Fire Technol.* **2022**, *59*, 473–496. [[CrossRef](#)]
9. Yu, M.; Yuan, H.; Li, K.; Wang, J. Research on multi-detector real-time fire alarm technology based on signal similarity. *Fire Saf. J.* **2022**, *136*, 103724. [[CrossRef](#)]
10. Milke, J.A.; Mcavoy, T.J. Analysis of Fire And Non-fire Signatures For Discriminating Fire Detection. *Fire Saf. Sci.* **1997**, *5*, 819–828. [[CrossRef](#)]
11. Solórzano, A.; Eichmann, J.; Fernández, L.; Ziems, B.; Jiménez-Soto, J.M.; Marco, S.; Fonollosa, J. Early fire detection based on gas sensor arrays: Multivariate calibration and validation. *Sens. Actuators B Chem.* **2022**, *352*, 130961. [[CrossRef](#)]
12. Andrew, A.M.; Shakaff, A.; Zakaria, A.; Gunasagaran, R.; Kanagaraj, E.; Saad, S.M. Early Stage Fire Source Classification in Building using Artificial Intelligence. In Proceedings of the 2018 IEEE Conference on Systems, Process and Control (ICSPC), Melaka, Malaysia, 14–15 December 2018; pp. 165–169. [[CrossRef](#)]
13. Bukowski, R.W.; Peacock, R.D.; Averill, J.D.; Cleary, T.G.; Bryner, N.P.; Reneke, P.A. *Performance of Home Smoke Alarms, Analysis of the Response of Several Available Technologies in Residential Fire Settings*; Technical Note 1455-1 (December 2007 Revision); NIST: Gaithersburg, MD, USA, 2003; pp. 5–8.
14. Nazir, A.; Mosleh, H.; Takruri, M.; Jallad, A.H.; Alhebsi, H. Early Fire Detection: A New Indoor Laboratory Dataset and Data Distribution Analysis. *Fire* **2022**, *5*, 11. [[CrossRef](#)]
15. Gottuk, D.T.; Peatross, M.J.; Roby, R.J.; Beyler, C.L. Advanced fire detection using multi-signature alarm algorithms. *Fire Saf. J.* **2002**, *37*, 381–394. [[CrossRef](#)]
16. Nakip, M.; Güzeliş, C. Multi-Sensor Fire Detector based on Trend Predictive Neural Network. In Proceedings of the 2019 11th International Conference on Electrical and Electronics Engineering (ELECO), Bursa, Turkey, 28–30 November 2019; pp. 600–604. [[CrossRef](#)]
17. Chen, S.J.; Hovde, D.C.; Peterson, K.A.; Marshall, A.W. Fire detection using smoke and gas sensors. *Fire Saf. J.* **2007**, *42*, 507–515. [[CrossRef](#)]

18. Gutmacher, D.; Hoefler, U.; Wöllenstein, J. Gas sensor technologies for fire detection. *Sens. Actuators B Chem.* **2012**, *175*, 40–45. [[CrossRef](#)]
19. Guo, S.; Yang, R.; Zhang, H.; Zhang, X. New Inverse Model for Detecting Fire-Source Location and Intensity. *J. Thermophys. Heat Transf.* **2010**, *24*, 745–755. [[CrossRef](#)]
20. Kou, L.; Wang, X.; Guo, X.; Zhu, J.; Zhang, H. Deep learning based inverse model for building fire source location and intensity estimation. *Fire Saf. J.* **2021**, *121*, 103310. [[CrossRef](#)]
21. Fonollosa, J.; Solórzano, A.; Marco, S. Chemical Sensor Systems and Associated Algorithms for Fire Detection: A Review. *Sensors* **2018**, *18*, 553. [[CrossRef](#)] [[PubMed](#)]
22. Alessandri, A.; Bagnerini, P.; Gaggero, M.; Mantelli, L. Parameter estimation of fire propagation models using level set methods. *Appl. Math. Model.* **2021**, *92*, 731–747. [[CrossRef](#)]
23. Krüger, S.; Despinasse, M.C.; Raspe, T.; Nörthemann, K.; Moritz, W. Early fire detection: Are hydrogen sensors able to detect pyrolysis of house hold materials? *Fire Saf. J.* **2017**, *91*, 1059–1067. [[CrossRef](#)]
24. Hayashi, Y.; Akimoto, Y.; Hiramatsu, N.; Masunishi, K.; Saito, T.; Yamazaki, H.; Nakamura, N.; Kojima, A. Smoldering Fire Detection Using Low-Power Capacitive MEMS Hydrogen Sensor for Future Fire Alarm. In Proceedings of the 2021 21st International Conference on Solid-State Sensors, Actuators and Microsystems (Transducers), Orlando, FL, USA, 20–24 June 2021; pp. 267–270. ISSN 2167-0021. [[CrossRef](#)]
25. Gutmacher, D.; Foelml, C.; Vollenweider, W.; Hoefler, U.; Wöllenstein, J. Comparison of gas sensor technologies for fire gas detection. *Procedia Eng.* **2011**, *25*, 1121–1124. [[CrossRef](#)]
26. DataSheet-GGS-6530-T\_Rev2203. 2023; pp. 1–2. Available online: [https://www.umweltsensortechnik.de/fileadmin/assets/downloads/gassensoren/single/DataSheet-GGS-6530-T\\_Rev2203.pdf](https://www.umweltsensortechnik.de/fileadmin/assets/downloads/gassensoren/single/DataSheet-GGS-6530-T_Rev2203.pdf) (accessed on 17 July 2023).
27. Carbon-Monoxide-Gas-Sensor\_Datasheet, 2023. Available online: <https://www.membrapor.ch/sheet/Carbon-Monoxide-Gas-Sensor-CO-MF-1000.pdf> (accessed on 17 July 2023).
28. Mostafa, E.; Nannen, C.; Henseler, J.; Diekmann, B.; Gates, R.; Buescher, W. Physical properties of particulate matter from animal houses—Empirical studies to improve emission modelling. *Environ. Sci. Pollut. Res.* **2016**, *23*, 12253–12263. [[CrossRef](#)]
29. Bin, H.; Yang, Y.; Cai, L.; Yuan, Z.; Roszak, S.; Yang, L. Experimental study on particles agglomeration by chemical and turbulent agglomeration before electrostatic precipitators. *Powder Technol.* **2018**, *335*, 186–194. [[CrossRef](#)]
30. Evtugina, M.; Alves, C.; Calvo, A.; Nunes, T.; Tarelho, L.; Duarte, M.; Prozil, S.O.; Evtuguin, D.V.; Pio, C. VOC emissions from residential combustion of Southern and mid-European woods. *Atmos. Environ.* **2014**, *83*, 90–98. [[CrossRef](#)]
31. Kim Oanh, N.T.; Ly, B.T.; Tipayarom, D.; Manandhar, B.R.; Prapat, P.; Simpson, C.D.; Sally Liu, L.J. Characterization of particulate matter emission from open burning of rice straw. *Atmos. Environ.* **2011**, *45*, 493–502. [[CrossRef](#)]
32. Cofer, W.R., III; Winstead, E.L.; Stocks, B.J.; Goldammer, J.G.; Cahoon, D.R. Crown fire emissions of CO<sub>2</sub>, CO, H<sub>2</sub>, CH<sub>4</sub>, and TNMHC from a dense Jack pine boreal forest fire. *Geophys. Res. Lett.* **1998**, *25*, 3919–3922. [[CrossRef](#)]
33. Kohl, D.; Kelleter, J.; Petig, H. Detection of Fires by Gas Sensors. *Sens. Update* **2001**, *9*, 161–223. .:1<161::AID-SEUP161>3.0.CO;2-A. [[CrossRef](#)]
34. Kropotova, S.S.; Kuznetsov, G.V.; Strizhak, P.A. Identifying products of pyrolysis and combustion of materials at incipient stages of fires. *Fire Saf. J.* **2022**, *132*, 103643. [[CrossRef](#)]
35. Vasiliev, A.A.; Grigoriev, G.Y.; Lagutin, A.S.; Nabiev, S.S.; Pislakov, A.V.; Samotaev, N.N.; Sokolov, A.V. Contemporary technologies of early detection of fire in space vehicles. *Acta Astronaut.* **2017**, *135*, 76–82. [[CrossRef](#)]

**Disclaimer/Publisher’s Note:** The statements, opinions and data contained in all publications are solely those of the individual author(s) and contributor(s) and not of MDPI and/or the editor(s). MDPI and/or the editor(s) disclaim responsibility for any injury to people or property resulting from any ideas, methods, instructions or products referred to in the content.